Published in final edited form as:
J Comp Neurol. 2012 December 1; 520(17): 3933–3948. doi:10.1002/cne.23137.

Melanocortin-4 Receptor Expression in Different Classes of Spinal and Vagal Primary Afferent Neurons in the Mouse

Laurent Gautron*, **Charlotte E. Lee**, **Syann Lee**, and **Joel K. Elmquist**
Department of Internal Medicine, Division of Hypothalamic Research, University of Texas Southwestern Medical Center, Dallas, Texas 75390-9077

Abstract

Melanocortin-4 receptor (MC4R) ligands are known to modulate nociception, but the site of action of MC4R signaling on nociception remains to be elucidated. The current study investigated MC4R expression in dorsal root ganglia (DRG) of the MC4R-GFP reporter mouse. Because MC4R is known to be expressed in vagal afferent neurons in the nodose ganglion (NG), we also systematically compared MC4R-expressing vagal and spinal afferent neurons. Abundant green fluorescent protein (GFP) immunoreactivity was found in about 45% of DRG neuronal profiles (at the mid-thoracic level), the majority being small-sized profiles. Immunohistochemistry combined with in situ hybridization confirmed that GFP was genuinely produced in MC4R-expressing neurons in the DRG. While a large number of GFP profiles in the DRG coexpressed Nav1.8 mRNA (84%) and bound isolectin B4 (72%), relatively few GFP profiles were positive for NF200 (16%) or CGRP (13%), suggesting preferential MC4R expression in C-fiber nonpeptidergic neurons. By contrast, GFP in the NG frequently colocalized with Nav1.8 mRNA (64%) and NF200 (29%), but only to a moderate extent with isolectin B4 (16%). Lastly, very few GFP profiles in the NG expressed CGRP (5%) or CART (4%). Together, our findings demonstrate variegated MC4R expression in different classes of vagal and spinal primary afferent neurons, and underscore the role of the melanocortin system in modulating nociceptive and nonnociceptive peripheral sensory modalities.

Keywords

Dorsal root ganglion; green fluorescent protein; neuropeptide; nociceptor; nodose ganglion; vagus nerve

Melanocortin-4 receptor (MC4R) signaling regulates a variety of functions in mammals including, most notably, energy balance and autonomic outflow (Cowley et al., 1999; Adage et al., 2001; Butler et al., 2001; Farooqi et al., 2003; Sutton et al., 2005; Tallam et al., 2006; Nogueiras et al., 2007; Krakoff et al., 2008; Greenfield et al., 2009; Skibicka and Grill, 2009), anxiety (Adan et al., 1999; Chaki et al., 2003), and several neuroendocrine systems (Fekete et al., 2000; Dhillo et al., 2002; Lu et al., 2003). Given its varied effects, it is not surprising that MC4R is widely expressed in the central and peripheral nervous systems. Prior anatomical mapping studies in rodents revealed MC4R expression in many hypothalamic, corticolimbic, and brainstem sites, as well as preganglionic and sensory

*CORRESPONDENCE TO: Laurent Gautron, Department of Internal Medicine, Division of Hypothalamic Research, University of Texas Southwestern Medical Center, 5323 Harry Hines Blvd., Dallas, TX 75390-9077. Laurent.Gautron@UTSouthwestern.edu.

Author contributions: Conception and design of experiments: L.G.; Collection and analysis of data: L.G., C.E.L., S.L.; Interpretation of data and critically revising the article: L.G., S.L., J.K.E.

autonomic neurons (Mountjoy et al., 1994; Kishi et al., 2003; Liu et al., 2003; Paues et al., 2006; Gautron et al., 2010).

Although the involvement of MC4R signaling in nociception has received little attention, there is emerging evidence that MC4R agonists are pronociceptive. For instance, the peripheral administration of melanotan II, an MC4R agonist, increases sensitivity to cold and mechanical pain in rats (Vrinten et al., 2000; Starowicz et al., 2002; Bertorelli et al., 2005). Conversely, the administration of the MC4R antagonist SHU9119 has potent antiallodynic effects. Although MC4R is present in brain sites important in pain processing such as the periaqueductal gray and reticular area (Kishi et al., 2003; Liu et al., 2003), the site(s) of action of MC4R signaling on nociception remains to be elucidated. However, the aforementioned modulatory effects of MC4R ligands on nociception are all recapitulated after their intrathecal delivery in the spinal cord (Vrinten et al., 2003; Starowicz et al., 2005), thus suggesting that MC4R could be present in spinal primary afferent terminals in the dorsal horn. In support of a direct action of MC4R in spinal primary afferents, two studies have detected MC4R transcripts by reverse-transcription polymerase chain reaction (RT-PCR) in the rodent dorsal root ganglion (DRG) (Starowicz et al., 2004; Tanabe et al., 2007).

Given all of the above observations, we reasoned that MC4R could be expressed in spinal primary afferent neurons in the DRG. However, the distribution and detailed anatomical characterization of MC4R in these neurons remained to be carried out. The present study investigated the distribution and phenotype of MC4R-expressing neurons in the mouse DRG using a unique MC4R-GFP reporter mouse model. In addition, double-labeling experiments with select presumptive markers for primary afferent neurons were performed. Because we previously reported MC4R expression in vagal afferent neurons in the nodose ganglion (NG) (Gautron et al., 2010), the present study systematically compares MC4R-expressing spinal afferent neurons to their vagal counterparts.

MATERIALS AND METHODS

Animals

Nine MC4R-GFP male mice between 2 and 4 months of age (≈25 g) were housed in a light-controlled (12/12 hours on/off; lights on at 6 AM) and temperature-controlled environment (21.5–22.5°C). As previously demonstrated by us (Liu et al., 2003; Gautron et al., 2010), MC4R-GFP mice faithfully express a blue-shifted green fluorescent protein (GFP) variant (Tau-Sapphire GFP) in MC4R-expressing neurons located in the central nervous system and peripheral ganglia. The maintenance and genotyping of the mice was performed as described before (Liu et al., 2003; Gautron et al., 2010). The procedures used in this study were approved by the University of Texas Southwestern Medical Center at Dallas Institutional Animal Care and Use Committees.

Tissue preparation

Mice were deeply anesthetized with chloral hydrate (500 mg/kg, intraperitoneally [i.p.]), and then perfused transcardially with 0.9% diethylpyrocarbonate (DEPC)-treated saline followed by 10% formalin (Sigma, St. Louis, MO). The left NG and DRG (both sides) were taken out with the help of a surgical scope, postfixed for 2 hours, and submerged in 20% sucrose overnight at 4°C. Tissue was embedded in OCT compound (Sakura, Torrance, CA) and frozen on dry ice. Sections were cut at 16 μm using a cryostat (1:5 series) collected on Superfrost slides (Fisherbrand, Pittsburgh, PA) and stored at −80°C until further processing.

Antibody characterization

The antisera used in the present study are all commercially available and their key features are summarized in Table 1.

Rabbit anti-GFP polyclonal antiserum (Invitrogen, La Jolla, CA): According to the manufacturer, this antibody detected GFP in a Microplate Dilution Assay. In addition, we have previously verified that this antibody only stained GFP-expressing neurons in the mouse (Scott et al., 2009; Gautron et al., 2010). Specifically, this antiserum produced no staining in wildtype mice, but stained GFP-expressing cells in the brain and NG of transgenic mice that express GFP. The present study further demonstrated that GFP immunoreactivity almost exclusively colocalized with MC4R mRNA in situ hybridization signal in the DRG of MC4R-GFP mice (Fig. 3), thus showing the specificity of the GFP staining.

Chicken anti-GFP polyclonal antiserum (Aves Laboratories, Tigard, OR): The manufacturer demonstrated that this antibody detected a single band of 28 kDa using western blot analysis. We also verified the specificity of this antibody in the mouse NG (Gautron et al., 2010), including the absence of staining after omitting the primary antiserum, and when used against wildtype tissue. In addition, we reported that GFP-expressing neurons in the NG of GFP reporter mice showed endogenous fluorescence (sapphire-GFP filter) that is only enhanced by immunostaining with the antiserum. The staining obtained using this antibody was cytoplasmic.

Rabbit polyclonal antiserum against calcitonin gene-related peptide (CGRP) (Bachem, Torrance, CA): Briefly, this antiserum recognizes canine, rat, and mouse α-CGRP and faithfully labels CGRP-expressing neurons in peripheral ganglia (Hall et al., 1997; Lennerz et al., 2008; Kosaras et al., 2009; Gautron et al., 2011). Controls for specificity included detection of one 4 kDa band corresponding to CGRP using western blot (Kosaras et al., 2009), and the absence of immunoreactivity in the presence of blocking peptide (Hall et al., 1997). CGRP immunoreactivity (using this antibody or others) has been reported in 20–50% of neuronal profiles in the mouse DRG depending on the anatomical level (Henken and Martin, 1992; Zwick et al., 2002; Price and Flores, 2007; Yamamoto et al., 2008; Tan et al., 2009). In the mouse NG, about 15–30% of the neurons are CGRP-positive (Ruan et al., 2004; Tan et al., 2009). It is noteworthy that it can be difficult to distinguish CGRP-positive neurons in the rostral pole of the NG from petrosal ganglion neurons, which often contain CGRP (Zhuo et al., 1997) and, hence, our CGRP profiles counts may include a few petrosal ganglion neurons.

Mouse monoclonal antibody (Sigma) against phosphorylated and nonphosphorylated neurofilament 200 (NF200): This antiserum is directed against the C-terminal segment of enzymatically dephosphorylated pig NF200. Fukuoka et al. (2008) validated the specificity of this antibody in the rat DRG. For instance, they demonstrated that it detected a single 200-kDA band, and preincubation with porcine NF200 (Chemicon, Temecula, CA) and omission of primary resulted in no staining. NF200 is mostly present in DRG neurons containing myelinated fibers including proprioceptors and low-threshold mechanoreceptors (Lawson et al., 1993; Fukuoka et al., 2008). In the mouse DRG, about 20–40% of the neuronal profiles are NF200-positive (Ruan et al., 2004; McGraw et al., 2005). While our current study identified 24% of neuronal profiles positive for NF200 in the NG, other reports range from 8–32% (Ruan et al., 2004; Staaf et al., 2010). NF200 immunoreactivity in our samples displayed a typical fiber-like appearance.

Rabbit polyclonal antiserum (Phoenix Pharmaceutical, Belmont, CA) against cocaine- and amphetamine-regulated transcript (CART): This antibody recognizes rat, mouse, and bovine

CART peptide fragment 55–102. Pre-adsorption with CART 55–102 peptide and omission of primary antibody both resulted in no staining (Dun et al., 2000; Cavalcante et al., 2006). Furthermore, western blot analysis of rat brain samples produced a single band of 5 kDa (manufacturer). This antibody was previously used to detect CART immunoreactivity in the rat NG (Zheng et al., 2002), and CART staining in our samples displayed a distribution pattern consistent with prior reports using this antiserum (Zheng et al., 2002; De Lartigue et al., 2010). The previous reports also demonstrated that roughly 50% of vagal afferents are CART-positive expressing vagal afferents represent of the ganglion neurons and include many CCK-sensitive neurons projecting to the gastrointestinal tract.

Immunohistochemistry (IHC)

Indirect immunoperoxidase technique—After washing in phosphate-buffered saline (PBS, pH 7.4), sections were pretreated with 0.3% hydrogen peroxide in PBS for 10 minutes at room temperature. Sections were incubated overnight in a rabbit anti-GFP polyclonal antiserum in 3% normal donkey serum (Jackson ImmunoResearch Laboratories, West Grove, PA) with 0.25% Triton X-100 in PBS (PBT). After several PBS rinses, sections were incubated in biotinylated donkey antirabbit (Jackson ImmunoResearch; cat. no. 711065152; lot no. 81161; 1:1,000), then incubated in a solution of ABC (Vectastain Elite ABC Kit; Vector Laboratories, Burlingame, CA; 1:1,000) dissolved in PBS for 1 hour. After washing in PBS, the sections were incubated in a solution of 0.04% diaminobenzidine tetrahydrochloride (DAB, Sigma) and 0.01% hydrogen peroxide (Aldrich Chemical, Milwaukee, WI). DAB-labeled sections were air-dried, dehydrated in graded ethanols, cleared in xylenes, and coverslipped with Permaslip (Alban Scientific, St. Louis, MO). GFP detection by immunoperoxidase staining was carried out in three MC4R-GFP mice.

Dual labeling fluorescent IHC—After several washes in PBS, sections were incubated overnight at room temperature in the anti-GFP chicken polyclonal antiserum in PBT with normal donkey serum (Jackson ImmunoResearch Laboratories) together with anti-CGRP, -NF200, or -CART (Table 1). After washing in PBS, sections were incubated in antichicken Alexa 488-conjugated secondary antibody (Invitrogen; cat. no. A11039; lot no. 488734; 1:1,000) for 1 hour at room temperature, then followed by Alexa 594-conjugated antirabbit (Invitrogen; cat. no. A21207; lot no. 404239; 1/1,000) or biotinylated-conjugated antimouse (Invitrogen; cat. no. 715065150; lot no. 85819; 1/1,000) secondary antibodies. The antimouse secondary was followed by Alexa 594-conjugated streptavidin (S32356; lot no. 830728; 1/1,000). Isolectin B4 (IB4) is commonly used to label nonpeptidergic C-fiber neurons (Fang et al., 2006). Sections were simultaneously incubated overnight at room temperature with primary anti-GFP chicken as described before and biotinylated-IB4 (Sigma; 5 mg/ml), followed by Alexa 594-conjugated streptavidin. IB4 binds to about 50% of murine DRG and NG neurons (Zwick et al., 2002; Ruan et al., 2004; Yamamoto et al., 2008; Tan et al., 2009). Fluorescently labeled tissue was washed and mounted on gelatin-coated slides, air-dried, and coverslipped with Vectashield mounting medium containing DAPI (Vector Laboratories; H-1500). Three MC4RGFP mice were used for the dual fluorescent IHC experiments.

MC4R and Nav1.8 in situ hybridization (ISH) combined with IHC

The MC4R antisense probe was made exactly as previously described (Gautron et al., 2010). Nav1.8 is a TTX-resistant voltage-gated sodium channel important in pain (Akopian et al., 1996; Laird et al., 2002). In the DRG, Nav1.8 is expressed in virtually all C fiber neurons and subsets of low threshold A-mechanoreceptors (Djouhri et al., 2003; Fukuoka et al., 2008). About 75–82% of NG neurons also express Nav1.8 (Stirling et al., 2005; Gautron et al., 2011). The Nav1.8 probe was designed from GenBank sequence NM_009134, spanning nucleotide positions 5825–6229, and was made from PCR fragments amplified with Taq

DNA polymerase (Millipore, Bedford, MA) from cDNA generated with SuperScript III First-Strand Synthesis System for RT-PCR (Invitrogen) from total mouse brain RNA (Stratagene, La Jolla, CA). The primers used to clone the probe were: 1) Nav1F TGACAGGGCCAACATTAACA and 2) Nav2R ACCACCAGAAATGTCCTTGC. The PCR product was cloned with the TOPO TA Cloning Kit for Sequencing (Invitrogen). Antisense and sense ^{35}S labeled probes were generated with MAXIscript In Vitro Transcription Kits (Ambion, Austin, TX).

The procedure for ISH was performed as previously reported (Gautron et al., 2010). Briefly, sections were fixed in 4% formaldehyde in DEPC-treated PBS, pH 7.0 (20 min at 4°C), dehydrated in ethanol, cleared in xylene, and rehydrated in decreasing concentrations of ethanol. Sections were then incubated in sodium citrate buffer (95–100°C, pH 6.0) and microwaved for 10 minutes (70% power), dehydrated in graded ethanol, and air-dried. The ^{35}S-labeled cRNA probes were diluted to 10^6 cpm/ml in a hybridization solution containing 50% formamide, 10 mM Tris-HCl, pH 8.0, 5 mg tRNA (Invitrogen), 10 mM dithiothreitol (DTT), 10% dextran sulfate, 0.3 M NaCl, 1 mM EDTA, pH 8.0, and 1× Denhardt's solution. Hybridization solution and a coverslip were applied to each slide and sections were placed at 57°C for 12–16 hours. Afterwards, sections were washed with 2× SSC buffer and incubated in 0.002% RNase A (Roche Molecular Biochemicals, Indianapolis, IN) with 0.5 M NaCl, 10 mM Tris-HCl, pH 8.0, and 1 mM EDTA for 30 minutes, followed by a 30-minute incubation in the same buffer without the RNase. The sections were subsequently incubated in 2× SSC, 0.25% DTT at 50°C for 1 hour, in 0.2× SSC, 0.25% DTT at 55°C for 1 hour, in 0.2× SSC, 0.25% DTT at 60°C for 1 hour. Sections were rinsed with PBS and immunohistochemistry for GFP was performed as described above using the immunoperoxidase indirect technique. The DAB staining was optimized by incubating the slides for 2 days with diluted rabbit primary antiserum (1/10,0000). Slides were air-dried, placed in x-ray film cassettes with BMR-2 film (Kodak, Rochester, NY) for 3 days, and then dipped in NTB2 photographic emulsion (Kodak) at 4°C for 2 weeks. Finally, slides were developed with D-19 developer (Kodak), dehydrated in graded ethanols, cleared in xylenes, and coverslipped with Permaslip (Alban Scientific). Three MC4R-GFP mice were used for combined ISH/IHC experiments.

Profile counts

Profiles counts methods are admittedly biased, as they do not allow for the determination of the true number of neurons in a particular structure (Coggeshall and Lekan, 1996). Nonetheless, profile counting was chosen because we were only interested in the proportion of neuronal profiles being positive for a specific marker rather than the absolute numbers of neurons being positive for the markers of interest. The following steps were taken to reduce counting biases: 1) only nucleated profiles were taken into account; 2) evenly spaced series of sections (1 in 5) from three entire ganglia (NG and DRG) from three different mice were used for quantitative analysis; 3) a large number of profiles was sampled and correction factors were applied when necessary (see below). Once again, this approach provides relative data that are not meant to be accurate estimates of absolute cell counts.

The surface area (in μm^2) of individual thoracic GFP-positive neuronal profiles was measured using Zeiss Axiovision 4.7 software. Counting of GFP-positive neuronal profiles was performed on fluorescently labeled and DAPI-counterstained sections. Of note, large profiles tend to be overrepresented and our counts were corrected using the Abercrombie formula as follows:

$$N = (n * T) / (T+D)$$

Where N = corrected number of profiles; n = counted number of profiles; T = sections thickness; D = mean neuronal diameter bin. The size of profiles was expressed in frequency (%) and appeared normally distributed compared to other studies on the mouse DRG using biased or unbiased profiles counting (Brumovsky et al., 2005; Tan et al., 2009).

We also estimated the proportion of GFP-profiles expressing MC4R or Nav1.8 mRNA, as well as displaying CGRP, NF200, and IB4 staining. Double fluorescence data are represented as percentages of counted profiles positive for GFP alone or in combination with select markers (mean ± SEM, $n = 3$). Cautiously, we were reluctant to directly compare our ISH/IHC with double fluorescence experiments as it is possible that ISH and IHC combined together can reduce the efficacy of both procedures. Thionin-counterstained profiles were considered to express MC4R or Nav1.8 mRNA only if silver grains above background conformed to the shape of identified GFP profiles. Cells with only weak DAB staining or uncertain hybridization signal were excluded. Combined ISH/IHC data are only represented as percentages of GFP-profiles expressing selected mRNA (mean ± SEM, $n = 3$). The Abercrombie formula was not applied to our double-labeling counts because the size of counted profiles was not taken into consideration.

Production of digital images

DAB-stained and ISH materials were analyzed using a Zeiss microscope Axioimager Z1 using brightfield optics. Digital images were captured using a digital camera (Axiocam) attached to the microscope and a desktop computer running the Axiovision 4.7 software. A camera lucida attached to the microscope was used to draw double-labeled cells for GFP and Nav1.8 mRNA. High-resolution fluorescent images were generated using stacks of optical sections (between 4 and 6 sections, step of 0.8–1.5 μm) obtained with a Zeiss microscope Imager ZI attached to the Apotome system. Images were captured with a black and white digital camera (Axiocam) attached to the microscope and a desktop computer running Axiovision 4.5. Optical sections obtained in three different channels (GFP, CY3, and DAPI filters) were digitally merged and the GFP-CY3-DAPI channels were converted to red-green-white. Magenta-green versions are provided for the assistance of color-blind readers. Of note, images used for quantitative estimates were captured under standardized exposure settings. Photoshop CS2 (Adobe, San Jose, CA) was used to make annotations, combine drawings and digital images into plates, and adjust the contrast and brightness of images.

RESULTS

GFP distribution in the mouse DRG

GFP IHC was used to systematically identify MC4R-expressing neurons in the DRG of MC4R-GFP reporter mice (Fig. 1A–E). Robust GFP immunoreactivity was observed in the cytoplasm of many DRG neurons (Fig. 1A–E). The distribution of GFP appeared comparable throughout the entire extent of the spinal cord from the cervical to lumbar level (Fig. 1A–D). As a note, our analyses from here onward were conducted in the mid-thoracic DRG only (T4–T6). Thoracic DRG neurons were chosen because they are known to innervate visceral tissues more substantially, and therefore are more directly comparable to NG neurons in terms of functions and innervated targets. We found that 45.0 ± 1.7% (out of 7,586 profiles, $n = 3$) of thoracic DRG neuronal profiles were positive for GFP. Interestingly, GFP-positive profiles were mostly, but not exclusively, represented by small-sized profiles (Fig. 2). For comparison, GFP-positive profiles in the NG represented 32.6 ± 0.4% (out of 3,109 profiles, $n = 3$; see also Gautron et al., 2010). MC4R mRNA ISH followed by GFP IHC was performed in order to evaluate the respective distribution patterns of MC4R mRNA and GFP immunoreactivity (Fig. 3A,B). These double-labeling experiments showed that 98.3 ± 0.9% (out of 100 GFP profiles; $n = 3$) of GFP-positive

profiles at the thoracic level also showed silver grain accumulation (Fig. 3B), and hence GFP was genuinely present in DRG MC4R-expressing neurons. A similar control experiment for MC4R-expressing NG neurons was included in a previous publication (Gautron et al., 2010).

Phenotyping of spinal and vagal GFP-positive profiles

Combined ISH/IHC labeling was conducted to determine the proportion of GFP profiles that coexpressed Nav1.8 mRNA in the DRG and NG. As anticipated, Nav1.8 mRNA was present in a large number of neurons in both sensory ganglia (Fig. 4). Hybridization with the corresponding sense probe produced no detectable signal (Fig. 4B). A high degree of colocalization between Nav1.8 mRNA and GFP was observed in the thoracic DRG (Fig. 4 D,F). Based on our observations, 84.3 ± 2.9% (out of 253 GFP profiles, $n = 3$) of GFP-positive profiles coexpressed Nav1.8 mRNA. Notably, Nav1.8 mRNA also extensively colocalized with GFP in the NG with about 67.7 ± 6.7% (out of 200 profiles, $n = 3$) of GFP profiles coexpressing Nav1.8 mRNA (Fig. 4C,E; Table 2).

In order to further narrow down the identity of GFP-positive profiles, we conducted double fluorescent labeling experiments with CGRP and IB4 which identify C-fiber peptidergic vs. nonpeptidergic neurons in the DRG, respectively (Snider and McMahon, 1998). Relatively few GFP profiles colocalized with CGRP in both the DRG (13.4%) and NG (4.2%) (Fig. 5; Table 2). Surprisingly, colocalization with IB4 revealed a different pattern of MC4R expression in the two sensory ganglia. In the DRG, as many as 72% of GFP profiles bound IB4 (Fig. 6A,C,E; Table 2), suggesting a predominant C-fiber nonpeptidergic phenotype consistent with our double-labeling experiments with Nav1.8 mRNA. By contrast, only 16.7% of GFP profiles bound IB4 in the NG (Fig. 6B,D,F; Table 2). Double-labeling experiments with NF200, a marker of myelinated A-fiber neurons in the DRG (see Materials and Methods), were then conducted. While a rather small proportion of neurons in the DRG were NF200-positive (16%) (Fig. 7A,C,E; Table 2), a larger proportion of GFP profiles coexpressed NF200 in the NG (29%) (Fig. 7B,D,F; Table 2). Because many of the GFP-positive vagal afferents could not be categorized using classical anatomical markers for DRG neurons, we reasoned that GFP could be present in a neurochemical type specific for vagal neurons. For example, CART is abundantly expressed in the NG but nearly absent in the DRG (Broberger et al., 1999; Zheng et al., 2002). However, less than 4% of GFP profiles in the NG expressed CART (Fig. 8A–C; Table 2).

DISCUSSION

Our results show that: 1) MC4R expression in the mouse DRG is found predominantly in, but not limited to, presumptive nociceptors which also express Nav1.8 and bind IB4; 2) MC4R-expressing vagal afferent neurons are comprised mainly of Nav1.8-expressing neurons and NF200-positive neurons, but few IB4- or neuropeptide-positive neurons. Collectively, our anatomical findings suggest that MC4R signaling in peripheral ganglia is implicated in a wide range of nociceptive and nonnociceptive peripheral sensory modalities.

Technical considerations

The use of transgenic MC4R-GFP mice allows for the straightforward anatomical analysis of MC4R-expressing neurons in the peripheral ganglia. Comparatively, the detection of MC4R-expressing neurons using MC4R mRNA ISH is a far more cumbersome approach. While this transgenic approach is limited to mice, the MC4R expression pattern is very similar between species (Mountjoy, 2010) and one can reasonably expect that our findings may apply to other animal species. Of note, we found that the GFP produced in DRG neurons did not appear to be effectively transported far from the cell body, for instance, to

peripheral tissues or the dorsal horn (not shown). This is in contrast with GFP-expressing vagal afferents that were shown to effectively transport GFP to their peripheral terminals (Gautron et al., 2010). In fact, more GFP-labeled axons can be seen in our NG compared to DRG samples (Figs. 5–8). The reason for the difference between the two types of ganglion is unknown.

It is important to keep in mind that, while anatomical criteria (size and immunohistochemical markers) have been widely used and proven useful for distinguishing major classes of primary sensory neurons (Brumovsky et al., 2005; Fukuoka et al., 2008; Scherrer et al., 2010), the classification of DRG neurons based on anatomical criteria alone is always oversimplistic. For instance, markers employed in this study showed some degree of overlap in DRG neurons (Fang et al., 2006; Price and Flores, 2007). Vagal afferent neurons display an even broader spectrum of functional properties that are not adequately reflected by anatomical criteria (Zhuo et al., 1997; Czaja et al., 2006; Fox, 2006). For example, in this study very few vagal GFP-profiles colocalized with IB4, CART, or CGRP, and yet these markers combined together accounted for almost the entire ganglion.

Functional significance of MC4R expression in DRG neurons

This study provides evidence that many DRG neurons express MC4R, a number of which are presumptive nonpeptidergic nociceptors. Our interpretation is based on the frequent expression of Nav1.8 mRNA in these neurons as well as their ability to bind IB4. It is well accepted that this category of DRG neurons (Nav1.8 and IB4) includes many C-fiber nociceptors that respond to mechanical and thermal noxious stimuli (Djouhri et al., 2003; Fang et al., 2006; Abrahamsen et al., 2008). These results are also agreement with pharmacological studies showing that MC4R ligands specifically modulate mechanical and thermal pain (Vrinten et al., 2000; Bertorelli et al., 2005; Starowicz et al., 2005). It will be interesting to test whether MC4R knockout mice display a pain phenotype independent of their obesity and late-onset diabetes phenotype.

The most likely source of ligands to MC4R located in DRG neurons is a descending hypothalamic input to the spinal cord from alpha-melanocyte stimulating hormone (α-MSH) neurons. This is based on the following observations: 1) α-MSH immunoreactive fibers have been reported in the rat spinal cord near the central canal and dorsal horn (Tsou et al., 1986), as well as the mouse spinal cord (Broberger et al., 1998); 2) binding of radioactive α-MSH within the dorsal horn (Lichtensteiger et al., 1996); 3) the intrathecal delivery of α-MSH exerts pronociceptive actions (Starowicz et al., 2005); 4) certain POMC neurons in the retrochiasmatic area and arcuate nucleus of the hypothalamus directly send projections to the spinal cord (Swanson and Kuypers, 1980; Elias et al., 1998). Together, these observations imply that MC4R may be transported to the presynaptic compartment of DRG neurons within the dorsal horn where it binds locally released α-MSH originating from the hypothalamus. A similar mechanism has been proposed to explain MC4R signaling in presynaptic vagal afferent terminals within the dorsovagal complex (Wan et al., 2008).

Importantly, the central melanocortin system is deeply implicated in the regulation of energy balance, and hence MC4R signaling in spinal afferents may provide a functional link between energy balance and nociception. In fact, obesity and food restriction have been demonstrated to influence pain thresholds. Despite some confounding factors (e.g., neuropathy and skin thickness in the obese), it is generally accepted that obesity enhances pain sensitivity in humans and rats (McKendall and Haier, 1983; Roane and Porter, 1986). Conversely, caloric restriction in mice exerts antinociceptive effects (Hargraves and Hentall, 2005). Changing levels of endogenous opioids in response to obesity and fasting have been long suspected to be implicated in linking energy balance to pain (de los Santos-Arteaga et al., 2003). The present data suggest an additional and complementary mechanism involving

the central melanocortin system. Such a mechanism could be speculated to dampen pain during periods of starvation to facilitate risky and food-seeking behaviors. Taken together, these observations underscore the importance of MC4R signaling as a promising target in the treatment of abnormal pain. Of note, small-diameter spinal afferent fibers are not exclusively involved in pain transmission, but also convey information relevant to the physiological conditions of innervated tissues (Craig et al., 2001).

Functional significance of MC4R expression in the NG

As previously mentioned, the categorization of vagal afferent neurons based on anatomical criteria is complicated due to their inherent heterogeneity. Here we show that about 30% of GFP-profiles in the NG included neurofilament-positive neurons that are regarded as A-fiber neurons. Ultrastructural and electrophysiological studies actually established that less than 10% of NG neurons correspond to A-fiber neurons in rabbits and cats (Agostoni et al., 1957; Stansfeld and Wallis, 1985). In addition, the reliability of NF200 as a marker for vagal A-neurons is questionable, as NF200-positive neurons in the NG sometimes share C-fiber electrophysiological features (Bielefeldt et al., 2006). Regardless of the true categorization of these fibers, it is known that subgroups of NF200 neurons are mechanoreceptors for airways and the heart (Ricco et al., 1996; Chuaychoo et al., 2005; Kosta et al., 2010), and others are gastrointestinal fibers that do not respond to stretch (Bielefeldt et al., 2006). Thus, at least a subgroup of vagal MC4R-expressing sensory neurons may be A-mechanoreceptors.

Interestingly, at least 64% of vagal MC4R-expressing profiles coexpressed Nav1.8 mRNA. It is known that Nav1.8 segregates C-fiber neurons from most A-fiber neurons in the rat DRG (Djouhri et al., 2003; Fukuoka et al., 2008). Hence, assuming that Nav1.8 is similarly distributed in the NG, many vagal MC4R/Nav1.8-expressing neurons should theoretically be C-fiber neurons. However, the exact role of these neurons can only be speculated. Although vagal afferents are not traditionally viewed as nociceptors (Cervero, 1994), they are increasingly recognized as being able to detect noxious and inflammatory stimuli that can evoke feelings of unpleasantness (Nassenstein et al., 2010). Perhaps Nav1.8-expressing vagal neurons are implicated in the response to noxious stimuli in vagally innervated viscera. Alternatively, there is mounting evidence that TTX-resistant sodium currents are not exclusively implicated in noxious responses but also contribute to nonnoxious sensory modalities including smell and itch (Liu et al., 2010; Weiss et al., 2011) as well as cardiovascular functions (Blasius et al., 2011). One of our prior studies showed that vagal Nav1.8-expressing neurons project to the cardiovascular system and gastrointestinal tract and are mostly represented by chemoreceptors/polymodal receptors (i.e., mucosal intestinal receptors) rather than pure mechanoreceptors (e.g., intramuscular arrays, baroreceptors) (Gautron et al., 2011). It is therefore tempting to believe that vagal MC4R/Nav1.8-expressing neurons could be implicated in normal visceral and autonomic functions. Interestingly, we previously established that about 20% of the GFP profiles in the NG coexpressed cholecystokinin receptor 1 and were connected to the duodenum (Gautron et al., 2010). Anatomical, physiological, and calcium imaging studies have shown that many cholecystokinin-sensitive fibers correspond to C-fiber neurons innervating the gastroduodenal mucosa (Ritter and Ladenheim, 1985; Holzer, 1991).

In conclusion, the current anatomical study provides evidence that MC4R signaling may be implicated in diverse vagal and spinal sensory modalities. Additional pharmacological, genetic, and physiological studies are warranted to determine the exact role of MC4R-expressing sensory neurons in nociception, bronchorespiratory, cardiovascular, and ingestive functions.

Acknowledgments

We thank Drs. Carol Elias and Jose Donato (UT Southwestern Medical Center) for providing the CART antibody, Dr. Jeffrey Friedman (Columbia University) for providing the MC4R-GFP mice, and Dr. Pin Xu (UT Southwestern Medical Center) for comments on the article.

Grant sponsor: National Institutes of Health; Grant numbers: P01DK088761, R01DK53301, RL1DK081185; Grant sponsor: American Diabetes Association.

LITERATURE CITED

Abrahamsen B, Zhao J, Asante CO, Cendan CM, Marsh S, Martinez-Barbera JP, Nassar MA, Dickenson AH, Wood JN. The cell and molecular basis of mechanical, cold, and inflammatory pain. Science. 2008; 321:702–705. [PubMed: 18669863]

Adage T, Scheurink AJ, de Boer SF, de Vries K, Konsman JP, Kuipers F, Adan RA, Baskin DG, Schwartz MW, van Dijk G. Hypothalamic, metabolic, and behavioral responses to pharmacological inhibition of CNS melanocortin signaling in rats. J Neurosci. 2001; 21:3639–3645. [PubMed: 11331393]

Adan RA, Szklarczyk AW, Oosterom J, Brakkee JH, Nijenhuis WA, Schaaper WM, Meloen RH, Gispen WH. Characterization of melanocortin receptor ligands on cloned brain melanocortin receptors and on grooming behavior in the rat. Eur J Pharmacol. 1999; 378:249–258. [PubMed: 10493100]

Agostoni E, Chinnock JE, De Daly MB, Murray JG. Functional and histological studies of the vagus nerve and its branches to the heart, lungs and abdominal viscera in the cat. J Physiol. 1957; 135:182–205. [PubMed: 13398974]

Akopian AN, Sivilotti L, Wood JN. A tetrodotoxin-resistant voltage-gated sodium channel expressed by sensory neurons. Nature. 1996; 379:257–262. [PubMed: 8538791]

Bertorelli R, Fredduzzi S, Tarozzo G, Campanella M, Grundy R, Beltramo M, Reggiani A. Endogenous and exogenous melanocortin antagonists induce anti-allodynic effects in a model of rat neuropathic pain. Behav Brain Res. 2005; 157:55–62. [PubMed: 15617771]

Bielefeldt K, Zhong F, Koerber HR, Davis BM. Phenotypic characterization of gastric sensory neurons in mice. Am J Physiol Gastrointest Liver Physiol. 2006; 291:G987–997. [PubMed: 16728726]

Blasius AL, Dubin AE, Petrus MJ, Lim BK, Narezkina A, Criado JR, Wills DN, Xia Y, Moresco EM, Ehlers C, Knowlton KU, Patapoutian A, Beutler B. Hypermorphic mutation of the voltage-gated sodium channel encoding gene Scn10a causes a dramatic stimulus-dependent neurobehavioral phenotype. Proc Natl Acad Sci U S A. 2011; 108:19413–19418. [PubMed: 22087007]

Broberger C, Holmberg K, Kuhar MJ, Hokfelt T. Cocaine-and amphetamine-regulated transcript in the rat vagus nerve: a putative mediator of cholecystokinin-induced satiety. Proc Natl Acad Sci U S A. 1999; 96:13506–13511. [PubMed: 10557351]

Broberger C, Johansen J, Johansson C, Schalling M, Hokfelt T. The neuropeptide Y/agouti gene-related protein (AGRP) brain circuitry in normal, anorectic, and monosodium glutamate-treated mice. Proc Natl Acad Sci USA. 1998; 95:15043–15048. [PubMed: 9844012]

Brumovsky P, Stanic D, Shuster S, Herzog H, Villar M, Hokfelt T. Neuropeptide Y2 receptor protein is present in peptidergic and nonpeptidergic primary sensory neurons of the mouse. J Comp Neurol. 2005; 489:328–348. [PubMed: 16025447]

Butler AA, Marks DL, Fan W, Kuhn CM, Bartolome M, Cone RD. Melanocortin-4 receptor is required for acute homeostatic responses to increased dietary fat. Nat Neurosci. 2001; 4:605–611. [PubMed: 11369941]

Cavalcante JC, Bittencourt JC, Elias CF. Female odors stimulate CART neurons in the ventral premammillary nucleus of male rats. Physiol Behav. 2006; 88:160–166. [PubMed: 16687159]

Cervero F. Sensory innervation of the viscera: peripheral basis of visceral pain. Physiol Rev. 1994; 74:95–138. [PubMed: 8295936]

Chaki S, Ogawa S, Toda Y, Funakoshi T, Okuyama S. Involvement of the melanocortin MC4 receptor in stress-related behavior in rodents. Eur J Pharmacol. 2003; 474:95–101. [PubMed: 12909200]

Chuaychoo B, Hunter DD, Myers AC, Kollarik M, Undem BJ. Allergen-induced substance P synthesis in large-diameter sensory neurons innervating the lungs. J Allergy Clin Immunol. 2005; 116:325–331. [PubMed: 16083787]

Coggeshall RE, Lekan HA. Methods for determining numbers of cells and synapses: a case for more uniform standards of review. J Comp Neurol. 1996; 364:6–15. [PubMed: 8789272]

Cowley MA, Pronchuk N, Fan W, Dinulescu DM, Colmers WF, Cone RD. Integration of NPY, AGRP, and melanocortin signals in the hypothalamic paraventricular nucleus: evidence of a cellular basis for the adipostat. Neuron. 1999; 24:155–163. [PubMed: 10677034]

Craig AD, Krout K, Andrew D. Quantitative response characteristics of thermoreceptive and nociceptive lamina I spinothalamic neurons in the cat. J Neurophysiol. 2001; 86:1459–1480. [PubMed: 11535691]

Czaja K, Ritter RC, Burns GA. Vagal afferent neurons projecting to the stomach and small intestine exhibit multiple N-methyl-D-aspartate receptor subunit phenotypes. Brain Res. 2006; 1119:86–93. [PubMed: 16989781]

De Lartigue G, Dimaline R, Varro A, Raybould H, De la Serre CB, Dockray GJ. Cocaine- and amphetamine-regulated transcript mediates the actions of cholecystokinin on rat vagal afferent neurons. Gastroenterology. 2010; 138:1479–1490. [PubMed: 19854189]

de los Santos-Arteaga M, Sierra-Dominguez SA, Fontanella GH, Delgado-Garcia JM, Carrion AM. Analgesia induced by dietary restriction is mediated by the kappa-opioid system. J Neurosci. 2003; 23:11120–11126. [PubMed: 14657170]

Dhillo WS, Small CJ, Seal LJ, Kim MS, Stanley SA, Murphy KG, Ghatei MA, Bloom SR. The hypothalamic melanocortin system stimulates the hypothalamo-pituitary-adrenal axis in vitro and in vivo in male rats. Neuroendocrinology. 2002; 75:209–216. [PubMed: 11979051]

Djouhri L, Fang X, Okuse K, Wood JN, Berry CM, Lawson SN. The TTX-resistant sodium channel Nav1.8 (SNS/PN3): expression and correlation with membrane properties in rat nociceptive primary afferent neurons. J Physiol. 2003; 550(Pt 3):739–752. [PubMed: 12794175]

Dun NJ, Dun SL, Wong PY, Yang J, Chang J. Cocaine-and amphetamine-regulated transcript peptide in the rat epididymis: an immunohistochemical and electrophysiological study. Biol Reprod. 2000; 63:1518–1524. [PubMed: 11058560]

Elias CF, Lee C, Kelly J, Aschkenasi C, Ahima RS, Couceyro PR, Kuhar MJ, Saper CB, Elmquist JK. Leptin activates hypothalamic CART neurons projecting to the spinal cord. Neuron. 1998; 21:1375–1385. [PubMed: 9883730]

Fang X, Djouhri L, McMullan S, Berry C, Waxman SG, Okuse K, Lawson SN. Intense isolectin-B4 binding in rat dorsal root ganglion neurons distinguishes C-fiber nociceptors with broad action potentials and high Nav1.9 expression. J Neurosci. 2006; 26:7281–7292. [PubMed: 16822986]

Farooqi IS, Yeo GS, O'Rahilly S. Binge eating as a phenotype of melanocortin 4 receptor gene mutations. N Engl J Med. 2003; 349:606–609. author reply 606-609. [PubMed: 12908459]

Fekete C, Legradi G, Mihaly E, Tatro JB, Rand WM, Lechan RM. alpha-Melanocyte stimulating hormone prevents fasting-induced suppression of corticotropin-releasing hormone gene expression in the rat hypothalamic paraventricular nucleus. Neurosci Lett. 2000; 289:152–156. [PubMed: 10904142]

Fox EA. A genetic approach for investigating vagal sensory roles in regulation of gastrointestinal function and food intake. Auton Neurosci. 2006; 126–127:9–29.

Fukuoka T, Kobayashi K, Yamanaka H, Obata K, Dai Y, Noguchi K. Comparative study of the distribution of the alpha-subunits of voltage-gated sodium channels in normal and axotomized rat dorsal root ganglion neurons. J Comp Neurol. 2008; 510:188–206. [PubMed: 18615542]

Gautron L, Lee C, Funahashi H, Friedman J, Lee S, Elmquist J. Melanocortin-4 receptor expression in a vago-vagal circuitry involved in postprandial functions. J Comp Neurol. 2010; 518:6–24. [PubMed: 19882715]

Gautron L, Sakata I, Udit S, Zigman JM, Wood JN, Elmquist JK. Genetic tracing of Nav1.8-expressing vagal afferents in the mouse. J Comp Neurol. 2011; 519:3085–3101. [PubMed: 21618224]

Greenfield JR, Miller JW, Keogh JM, Henning E, Satterwhite JH, Cameron GS, Astruc B, Mayer JP, Brage S, See TC, Lomas DJ, O'Rahilly S, Farooqi IS. Modulation of blood pressure by central melanocortinergic pathways. N Engl J Med. 2009; 360:44–52. [PubMed: 19092146]

Hall AK, Ai X, Hickman GE, MacPhedran SE, Nduaguba CO, Robertson CP. The generation of neuronal heterogeneity in a rat sensory ganglion. J Neurosci. 1997; 17:2775–2784. [PubMed: 9092599]

Hargraves WA, Hentall ID. Analgesic effects of dietary caloric restriction in adult mice. Pain. 2005; 114:455–461. [PubMed: 15777870]

Henken DB, Martin JR. Herpes simplex virus infection induces a selective increase in the proportion of galanin-positive neurons in mouse sensory ganglia. Exp Neurol. 1992; 118:195–203. [PubMed: 1385205]

Holzer P. Capsaicin: cellular targets, mechanisms of action, and selectivity for thin sensory neurons. Pharmacol Rev. 1991; 43:143–201. [PubMed: 1852779]

Kishi T, Aschkenasi CJ, Lee CE, Mountjoy KG, Saper CB, Elmquist JK. Expression of melanocortin 4 receptor mRNA in the central nervous system of the rat. J Comp Neurol. 2003; 457:213–235. [PubMed: 12541307]

Kosaras B, Jakubowski M, Kainz V, Burstein R. Sensory innervation of the calvarial bones of the mouse. J Comp Neurol. 2009; 515:331–348. [PubMed: 19425099]

Kosta V, Guic MM, Aljinovic J, Sapunar D, Grkovic I. Immunohistochemical characteristics of neurons in nodose ganglia projecting to the different chambers of the rat heart. Auton Neurosci. 2010; 155:33–38. [PubMed: 20102794]

Krakoff J, Ma L, Kobes S, Knowler WC, Hanson RL, Bogardus C, Baier LJ. Lower metabolic rate in individuals heterozygous for either a frameshift or a functional missense MC4R variant. Diabetes. 2008; 57:3267–3272. [PubMed: 18835933]

Laird JM, Souslova V, Wood JN, Cervero F. Deficits in visceral pain and referred hyperalgesia in Nav1.8 (SNS/PN3)-null mice. J Neurosci. 2002; 22:8352–8356. [PubMed: 12351708]

Lawson SN, Perry MJ, Prabhakar E, McCarthy PW. Primary sensory neurones: neurofilament, neuropeptides, and conduction velocity. Brain Res Bull. 1993; 30:239–243. [PubMed: 7681350]

Lennerz JK, Ruhle V, Ceppa EP, Neuhuber WL, Bunnett NW, Grady EF, Messlinger K. Calcitonin receptor-like receptor (CLR), receptor activity-modifying protein 1 (RAMP1), and calcitonin gene-related peptide (CGRP) immunoreactivity in the rat trigeminovascular system: differences between peripheral and central CGRP receptor distribution. J Comp Neurol. 2008; 507:1277–1299. [PubMed: 18186028]

Lichtensteiger W, Hanimann B, Siegrist W, Eberle AN. Region- and stage-specific patterns of melanocortin receptor ontogeny in rat central nervous system, cranial nerve ganglia and sympathetic ganglia. Brain Res Dev Brain Res. 1996; 91:93–110.

Liu H, Kishi T, Roseberry AG, Cai X, Lee CE, Montez JM, Friedman JM, Elmquist JK. Transgenic mice expressing green fluorescent protein under the control of the melanocortin-4 receptor promoter. J Neurosci. 2003; 23:7143–7154. [PubMed: 12904474]

Liu Y, Abdel Samad O, Zhang L, Duan B, Tong Q, Lopes C, Ji RR, Lowell BB, Ma Q. VGLUT2-dependent glutamate release from nociceptors is required to sense pain and suppress itch. Neuron. 2010; 68:543–556. [PubMed: 21040853]

Lu XY, Barsh GS, Akil H, Watson SJ. Interaction between alpha-melanocyte-stimulating hormone and corticotropin-releasing hormone in the regulation of feeding and hypothalamo-pituitary-adrenal responses. J Neurosci. 2003; 23:7863–7872. [PubMed: 12944516]

McGraw J, Gaudet AD, Oschipok LW, Steeves JD, Poirier F, Tetzlaff W, Ramer MS. Altered primary afferent anatomy and reduced thermal sensitivity in mice lacking galectin-1. Pain. 2005; 114:7–18. [PubMed: 15733626]

McKendall MJ, Haier RJ. Pain sensitivity and obesity. Psychiatry Res. 1983; 8:119–125. [PubMed: 6574530]

Mountjoy KG. Distribution and function of melanocortin receptors within the brain. Adv Exp Med Biol. 2010; 681:29–48. [PubMed: 21222258]

Mountjoy KG, Mortrud MT, Low MJ, Simerly RB, Cone RD. Localization of the melanocortin-4 receptor (MC4-R) in neuroendocrine and autonomic control circuits in the brain. Mol Endocrinol. 1994; 8:1298–1308. [PubMed: 7854347]

Nassenstein C, Taylor-Clark TE, Myers AC, Ru F, Nandigama R, Bettner W, Undem BJ. Phenotypic distinctions between neural crest and placodal derived vagal C-fibres in mouse lungs. J Physiol. 2010; 588(Pt 23):4769–4783. [PubMed: 20937710]

Nogueiras R, Wiedmer P, Perez-Tilve D, Veyrat-Durebex C, Keogh JM, Sutton GM, Pfluger PT, Castaneda TR, Neschen S, Hofmann SM, Howles PN, Morgan DA, Benoit SC, Szanto I, Schrott B, Schurmann A, Joost HG, Hammond C, Hui DY, Woods SC, Rahmouni K, Butler AA, Farooqi IS, O'Rahilly S, Rohner-Jeanrenaud F, Tschop MH. The central melanocortin system directly controls peripheral lipid metabolism. J Clin Invest. 2007; 117:3475–3488. [PubMed: 17885689]

Paues J, Mackerlova L, Blomqvist A. Expression of melanocortin-4 receptor by rat parabrachial neurons responsive to immune and aversive stimuli. Neuroscience. 2006; 141:287–297. [PubMed: 16730913]

Price TJ, Flores CM. Critical evaluation of the colocalization between calcitonin gene-related peptide, substance P, transient receptor potential vanilloid subfamily type 1 immunoreactivities, and isolectin B4 binding in primary afferent neurons of the rat and mouse. J Pain. 2007; 8:263–272. [PubMed: 17113352]

Ricco MM, Kummer W, Biglari B, Myers AC, Undem BJ. Interganglionic segregation of distinct vagal afferent fibre phenotypes in guinea-pig airways. J Physiol. 1996; 496(Pt 2):521–530. [PubMed: 8910234]

Ritter RC, Ladenheim EE. Capsaicin pretreatment attenuates suppression of food intake by cholecystokinin. Am J Physiol. 1985; 248(4 Pt 2):R501–504. [PubMed: 3985191]

Roane DS, Porter JR. Nociception and opioid-induced analgesia in lean (Fa/-) and obese (fa/fa) Zucker rats. Physiol Behav. 1986; 38:215–218. [PubMed: 3797488]

Ruan HZ, Moules E, Burnstock G. Changes in P2X3 purinoceptors in sensory ganglia of the mouse during embryonic and postnatal development. Histochem Cell Biol. 2004; 122:539–551. [PubMed: 15549366]

Scherrer G, Low SA, Wang X, Zhang J, Yamanaka H, Urban R, Solorzano C, Harper B, Hnasko TS, Edwards RH, Basbaum AI. VGLUT2 expression in primary afferent neurons is essential for normal acute pain and injury-induced heat hypersensitivity. Proc Natl Acad Sci USA. 2010; 107:22296–22301. [PubMed: 21135246]

Scott MM, Lachey JL, Sternson SM, Lee CE, Elias CF, Friedman JM, Elmquist JK. Leptin targets in the mouse brain. J Comp Neurol. 2009; 514:518–532. [PubMed: 19350671]

Skibicka KP, Grill HJ. Hypothalamic and hindbrain melanocortin receptors contribute to the feeding, thermogenic, and cardiovascular action of melanocortins. Endocrinology. 2009; 150:5351–5361. [PubMed: 19854868]

Snider WD, McMahon SB. Tackling pain at the source: new ideas about nociceptors. Neuron. 1998; 20:629–632. [PubMed: 9581756]

Staaf S, Franck MC, Marmigere F, Mattsson JP, Ernfors P. Dynamic expression of the TRPM subgroup of ion channels in developing mouse sensory neurons. Gene Expr Patterns. 2010; 10:65–74. [PubMed: 19850157]

Stansfeld CE, Wallis DI. Properties of visceral primary afferent neurons in the nodose ganglion of the rabbit. J Neurophysiol. 1985; 54:245–260. [PubMed: 4031986]

Starowicz K, Przewlocki R, Gispen WH, Przewlocka B. Modulation of melanocortin-induced changes in spinal nociception by mu-opioid receptor agonist and antagonist in neuropathic rats. Neuroreport. 2002; 13:2447–2452. [PubMed: 12499847]

Starowicz K, Bilecki W, Sieja A, Przewlocka B, Przewlocki R. Melanocortin 4 receptor is expressed in the dorsal root ganglions and down-regulated in neuropathic rats. Neurosci Lett. 2004; 358:79–82. [PubMed: 15026153]

Starowicz K, Obara I, Przewlocki R, Przewlocka B. Inhibition of morphine tolerance by spinal melanocortin receptor blockade. Pain. 2005; 117:401–411. [PubMed: 16153779]

Stirling LC, Forlani G, Baker MD, Wood JN, Matthews EA, Dickenson AH, Nassar MA. Nociceptor-specific gene deletion using heterozygous NaV1.8-Cre recombinase mice. Pain. 2005; 113:27–36. [PubMed: 15621361]

Sutton GM, Duos B, Patterson LM, Berthoud HR. Melanocortinergic modulation of cholecystokinin-induced suppression of feeding through extracellular signal-regulated kinase signaling in rat solitary nucleus. Endocrinology. 2005; 146:3739–3747. [PubMed: 15961554]

Swanson LW, Kuypers HG. A direct projection from the ventromedial nucleus and retrochiasmatic area of the hypothalamus to the medulla and spinal cord of the rat. Neurosci Lett. 1980; 17:307–312. [PubMed: 7052476]

Tallam LS, da Silva AA, Hall JE. Melanocortin-4 receptor mediates chronic cardiovascular and metabolic actions of leptin. Hypertension. 2006; 48:58–64. [PubMed: 16754792]

Tan LL, Bornstein JC, Anderson CR. Neurochemical and morphological phenotypes of vagal afferent neurons inner-vating the adult mouse jejunum. Neurogastroenterol Motil. 2009; 21:994–1001. [PubMed: 19413682]

Tanabe K, Gamo K, Aoki S, Wada K, Kiyama H. Melanocortin receptor 4 is induced in nerve-injured motor and sensory neurons of mouse. J Neurochem. 2007; 101:1145–1152. [PubMed: 17286587]

Tsou K, Khachaturian H, Akil H, Watson SJ. Immunocytochemical localization of pro-opiomelanocortin-derived peptides in the adult rat spinal cord. Brain Res. 1986; 378:28–35. [PubMed: 3017502]

Vrinten DH, Gispen WH, Groen GJ, Adan RA. Antagonism of the melanocortin system reduces cold and mechanical allodynia in mononeuropathic rats. J Neurosci. 2000; 20:8131–8137. [PubMed: 11050135]

Vrinten DH, Gispen WH, Kalkman CJ, Adan RA. Interaction between the spinal melanocortin and opioid systems in a rat model of neuropathic pain. Anesthesiology. 2003; 99:449–454. [PubMed: 12883419]

Wan S, Browning KN, Coleman FH, Sutton G, Zheng H, Butler A, Berthoud HR, Travagli RA. Presynaptic melanocortin-4 receptors on vagal afferent fibers modulate the excitability of rat nucleus tractus solitarius neurons. J Neurosci. 2008; 28:4957–4966. [PubMed: 18463249]

Weiss J, Pyrski M, Jacobi E, Bufe B, Willnecker V, Schick B, Zizzari P, Gossage SJ, Greer CA, Leinders-Zufall T, Woods CG, Wood JN, Zufall F. Loss-of-function mutations in sodium channel Nav1.7 cause anosmia. Nature. 2011; 472:186–190. [PubMed: 21441906]

Yamamoto W, Sugiura A, Nakazato-Imasato E, Kita Y. Characterization of primary sensory neurons mediating static and dynamic allodynia in rat chronic constriction injury model. J Pharm Pharmacol. 2008; 60:717–722. [PubMed: 18498707]

Zheng H, Patterson LM, Berthoud HR. CART in the dorsal vagal complex: sources of immunoreactivity and effects on Fos expression and food intake. Brain Res. 2002; 957:298–310. [PubMed: 12445972]

Zhuo H, Ichikawa H, Helke CJ. Neurochemistry of the nodose ganglion. Prog Neurobiol. 1997; 52:79–107. [PubMed: 9185234]

Zwick M, Davis BM, Woodbury CJ, Burkett JN, Koerber HR, Simpson JF, Albers KM. Glial cell line-derived neurotrophic factor is a survival factor for isolectin B4-positive, but not vanilloid receptor 1-positive, neurons in the mouse. J Neurosci. 2002; 22:4057–4065. [PubMed: 12019325]

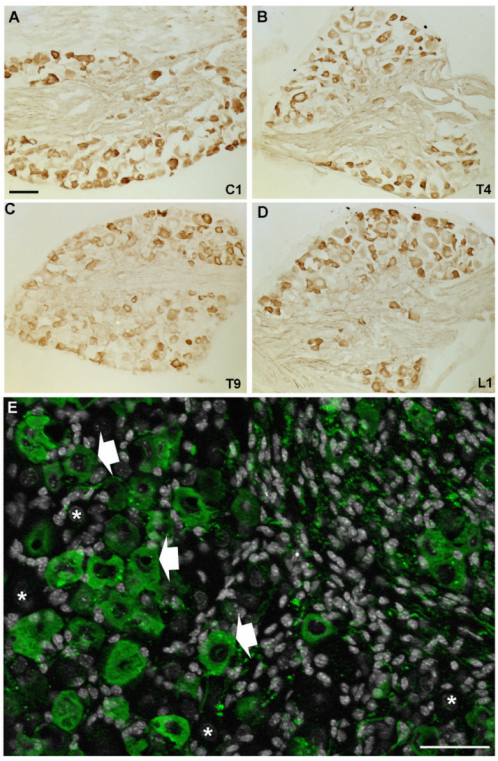

Figure 1.
Immunohistochemical labeling of GFP-positive profiles in the DRG of MC4R-GFP mice. DAB-labeled profiles were observed in DRG from all levels of the spinal cord that were studied (**A–D**) (brightfield). Anatomical levels indicated in bottom right corners. Higher magnification of DAPI-counterstained (white color) thoracic DRG reveals the morphological details of GFP-positive profiles (epifluorescence and Apotome) (**E**). Representative GFP-positive and -negative profiles are indicated by white arrows and asterisks, respectively. Scale bars = 100 μm in A–D; 50 μm in E.

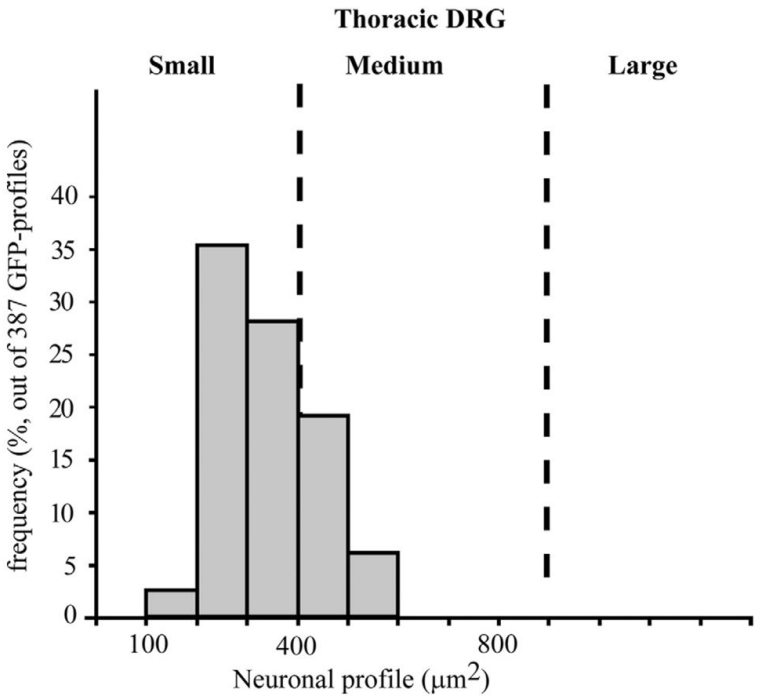

Figure 2.
Graph showing the size distribution of GFP-positive profiles in the thoracic DRG. Note that GFP-positive profiles are most often represented by small-sized profiles. Data are expressed in μm^2 and include observations pooled from 387 profiles. These data were corrected using the Abercrombie formula (see Materials and Methods).

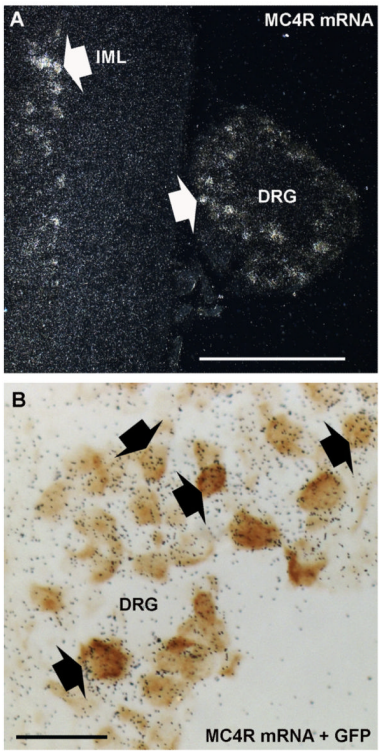

Figure 3.
Double ISH/IHC labeling for MC4R mRNA and GFP. White arrows indicate representative cells with visible ISH signal in the thoracic spinal cord and attached DRG (darkfield) (**A**). GFP-positive profiles (brown) are consistently overlaid by black silver grains, which indicate MC4R mRNA expression (brightfield) (**B**). Black arrows show examples of colocalization. IML, intermediolateral cell column. Scale bars = 500 μm in A; 50 μm in B.

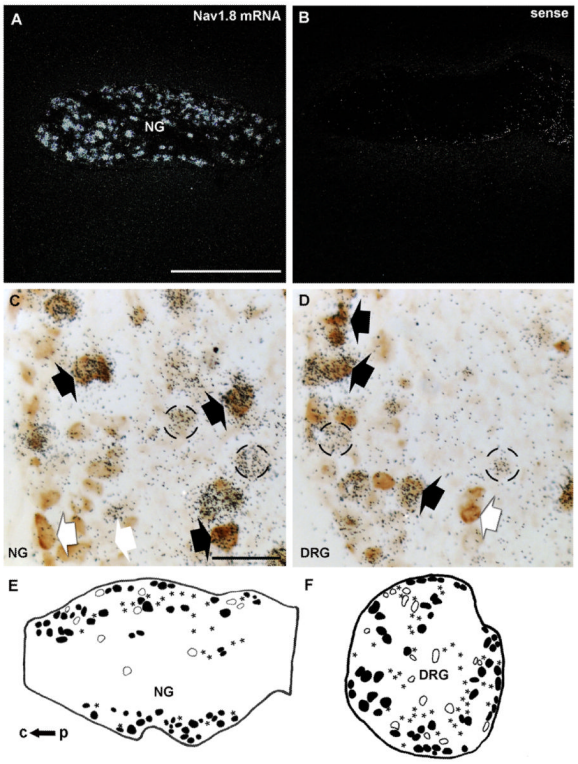

Figure 4.

Double ISH/IHC labeling for Nav1.8 mRNA and GFP. Robust hybridization signal (darkfield) for Nav1.8 mRNA is visible in the NG (**A**). By contrast, the sense probe reveals no significant signal (**B**). GFP-positive profiles (brown) are frequently overlaid by black silver grains, which indicate Nav1.8 mRNA expression in both the NG (**C**) and DRG (**D**). Black arrows show examples of double-labeled neurons, whereas white arrows show profiles solely GFP positive, and circles highlight Nav1.8-expressing cells only. Camera lucida drawings showing the typical distribution of profiles only positive for GFP (open profiles), only for Nav1.8 (asterisks), or double-labeled (black profiles) in a representative NG (**E**) and DRG (**F**). c, central end; p, peripheral end. Scale bars = 500 μm in A; 50 μm in C,D.

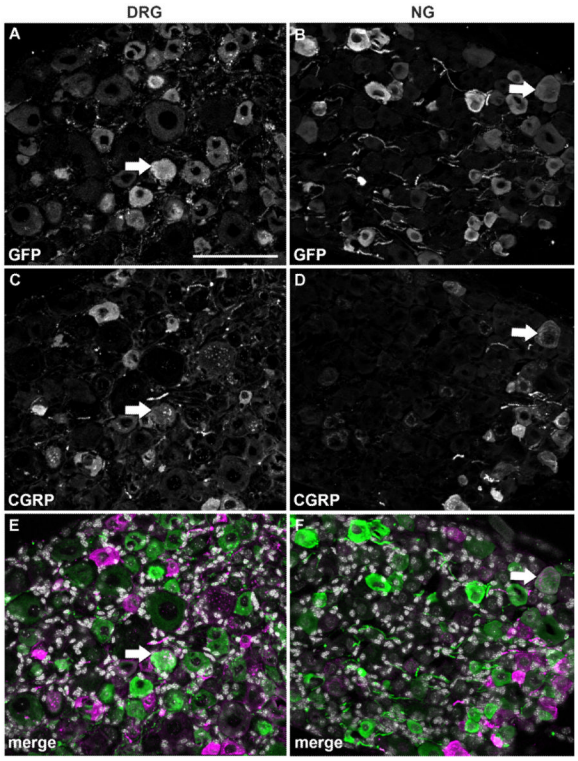

Figure 5.
Double immunolabeling for GFP and CGRP. Optical sections (epifluorescence and Apotome) of the DRG and NG double-labeled for GFP (**A,B**) and CGRP (**C,D**). DAPI staining appears in white in the merge color images (**E,F**). Note that double-labeled profiles (white arrows) are relatively rare in either ganglia. Scale bar = 100 μm (applies to all).

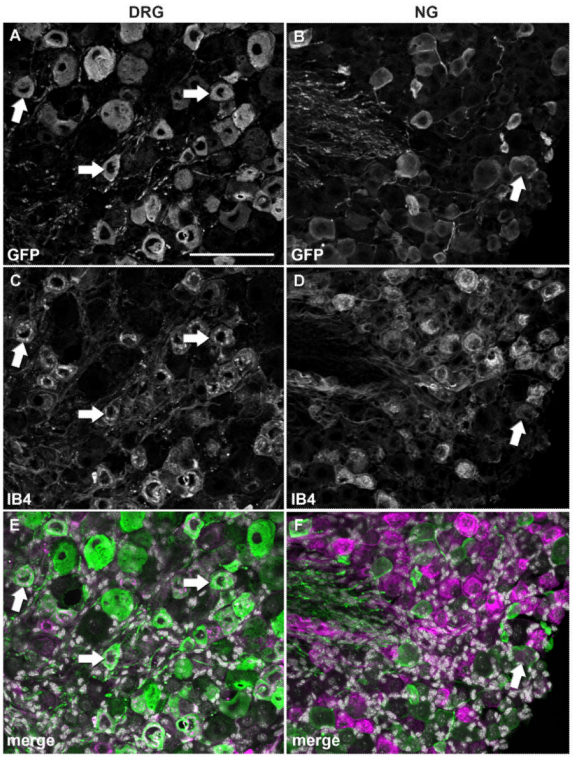

Figure 6.
Double immunolabeling for GFP and IB4. Optical sections (epifluorescence and Apotome) of the DRG and NG double-labeled for GFP (**A**,**B**) and IB4 (**C**,**D**). DAPI staining appears in white in the merge color images (**E**,**F**). Strikingly, double-labeled profiles are very frequent in the DRG (white arrows), but rare in the NG. Scale bar = 100 μm (applies to all).

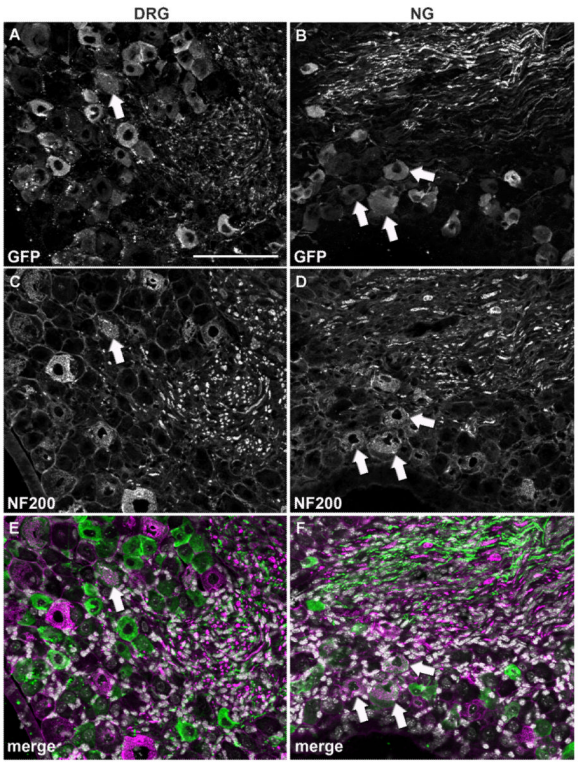

Figure 7.
Double immunolabeling for GFP and NF200. Optical sections (epifluorescence and Apotome) of the DRG and NG double-labeled for GFP (**A,B**) and NF200 (**C,D**). DAPI staining appears white in the merge color images (**E,F**). Although double-labeled profiles are observed in both ganglia (white arrows), they appear more frequently in the NG. Scale bar = 100 μm (applies to all).

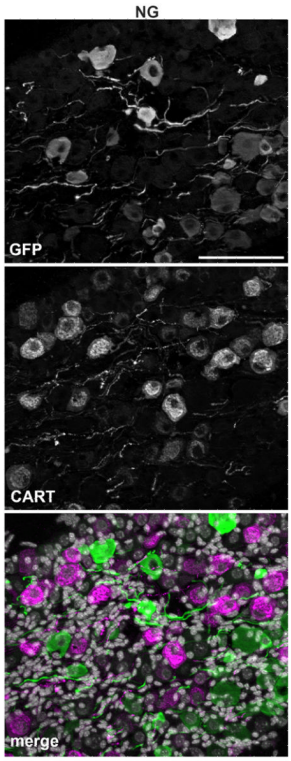

Figure 8.
Double immunolabeling for GFP and CART. Optical sections (epifluorescence and Apotome) of the NG double-labeled for GFP (**A**) and CART (**B**). Of note, CART-positive profiles are rare in the DRG (not shown). DAPI staining is white in the merged color images (**C**). Double-labeled profiles are not seen. Scale bar = 100 μm (applies to all).

TABLE 1

Primary Antisera

Antigen	Immunogen	Manufacturer	Dilution used
CART	Ile-Pro-Ile-Tyr-Glu-Lys-Lys-Tyr-Gly-Gln-Val-Pro-Met-Cys-Asp-Ala-Gly -Glu-Gln-Cys-Ala-Val-Arg-Lys-Gly-Ala-Arg-Ile- Gly-Lys-Leu-Cys-Asp-Cys-Pro-Arg-Gly-Thr-Ser-Cys-Asn-Ser-Phe-Leu-Leu-Lys-Cys-Leu [Disulfide bonds between Cys 1-Cys3,Cys 2-Cys5,Cys 4-Cys 6]	Phoenix Pharmaceuticals, cat. no. H-003-62, lot no. 01104, rabbit polyclonal	1/3,000
CGRP	H-Ser-Cys-Asn-Thr-Ala-Thr-Cys-Val-Thr-His-Arg-Leu-Ala-Gly-Leu-Leu-Ser-Arg-Ser-Gly-Gly-Val-Val-Lys-Asp-Asn-Phe-Val-Pro-Thr-Asn-Val-Gly-Ser-Glu-Ala-Phe-$NH2_2$	Peninsula Laboratories, cat. no. T4032, lot no. 040826-7, rabbit polyclonal	1/2,000
GFP	GFP purified from *Aequora Victoria*	Invitrogen, cat. no. A6455, lot no. 71B1, rabbit polyclonal	1/20,000
GFP	GFP emulsified in Freund's adjuvant	Aves Lab., cat. no. GFP-1020, lot no. 0425FP07, chicken polyclonal	1/2,000
NF200	C-terminal tail segment of dephosphorylated pig neurofilament H-subunit	Sigma, cat. no. N0142, lot no. 059K4785, mouse monoclonal.	1/2,000

TABLE 2

Phenotype of GFP Profiles Within Mouse Peripheral Ganglia

Marker	GFP$^+$/marker$^-$	GFP$^+$/marker$^+$ (marker/GFP)	GFP$^-$/marker$^+$	GFP−/marker−
IB4				
DRG (1686)	13 ± 1.2%	34.7 ± 0.2% (72.1 ± 2.5%)	12.2 ± 2.1%	40.1 ± 2.4%
NG (1185)	27.9 ± 0.4%	5.1 ± 0.3% (16.7 ± 0.6%)	40.1 ± 2.4%	21.7 ± 2.3%
CGRP				
DRG (1741)	39.7 ± 2.9%	6.2 ± 1.4% (13.4 ± 2.7%)	14.1 ± 1.4%	40 ± 3.2%
NG (1159)	32.5 ± 2.2%	1.8 ± 0.5% (4.2 ± 1.6%)	12.3 ± 1.8%	53.4 ± 0.1%
NF200				
DRG (1336)	34.6 ± 1.6%	8.8 ± 1.3% (16.7 ± 1.7%)	15.6 ± 1.2%	41 ± 2.7%
NG (988)	23.2 ± 2.7%	9.3 ± 1.1% (29.1 ± 4.4%)	14.3 ± 0.9%	53.2 ± 1.6%
CART				
NG (936)	30.9 ± 2.2%	1.4 ± 0.4% (4.3 ± 1.2)	39.5 ± 2.7	28.2 ± 4.6%

Marker	GFP$^+$/marker$^+$
MC4R mRNA	
DRG (100)	98.3 ± 0.9%
Nav1.8 mRNA	
DRG (253)	84.3 ± 2.9%
NG (200)	67.7 ± 6.7%

Mean percentages (±SEM, $n = 3$) of GFP profiles positive or negative for select markers of primary afferents within the thoracic DRG and left NG relative to the total number of sampled profiles. Data in the upper part of the table were obtained using double fluorescence labeling. The total number of profiles is indicated in parentheses in the first column. The proportion of GFP profiles positive for each marker is also indicated in parentheses in the middle column. Data in the bottom part of the table were obtained using combined ISH/IHC. Mean percentages (±SEM, $n = 3$) of GFP profiles positive for MC4R and Nav1.8 mRNA. The total number of examined GFP-profiles is indicated in parentheses in the first column. CART, cocaine- and amphetamine-regulated transcript; CGRP, calcitonin gene-related peptide; DRG, dorsal root ganglion; GFP, green fluorescent protein; IB4, isolectin B4; MC4R, melanocortin-4 receptor; NF200, neurofilament 200; NG, nodose ganglion.